



HAL
open science

Structural Determinants Underlying Photoprotection in the Photoactive Orange Carotenoid Protein of Cyanobacteria

Adjele Wilson, James N Kinney, Petrus H Zwart, Claire Punginelli, Sandrine d'Haene, Francois Perreau, Mickael G Klein, Diana Kirilovsky, Cheryl A Kerfeld

► To cite this version:

Adjele Wilson, James N Kinney, Petrus H Zwart, Claire Punginelli, Sandrine d'Haene, et al.. Structural Determinants Underlying Photoprotection in the Photoactive Orange Carotenoid Protein of Cyanobacteria. *Journal of Biological Chemistry*, 2010, 285 (24), pp.18364-18375. 10.1074/jbc.M110.115709 . hal-01203915

HAL Id: hal-01203915

<https://hal.science/hal-01203915v1>

Submitted on 31 May 2020

HAL is a multi-disciplinary open access archive for the deposit and dissemination of scientific research documents, whether they are published or not. The documents may come from teaching and research institutions in France or abroad, or from public or private research centers.

L'archive ouverte pluridisciplinaire **HAL**, est destinée au dépôt et à la diffusion de documents scientifiques de niveau recherche, publiés ou non, émanant des établissements d'enseignement et de recherche français ou étrangers, des laboratoires publics ou privés.

Copyright

Structural Determinants Underlying Photoprotection in the Photoactive Orange Carotenoid Protein of Cyanobacteria[§]

Received for publication, February 22, 2010, and in revised form, March 21, 2010. Published, JBC Papers in Press, April 5, 2010, DOI 10.1074/jbc.M110.115709

Adjele Wilson^{‡§1}, James N. Kinney^{¶2}, Petrus H. Zwart^{¶3}, Claire Punginelli^{‡§1}, Sandrine D'Haene^{‡§1}, François Perreau^{||}, Michael G. Klein^{¶2}, Diana Kirilovsky^{‡§1}, and Cheryl A. Kerfeld^{¶***2,4}

From the [‡]Commissariat à l'Energie Atomique, Institut de Biologie et Technologies de Saclay, and [§]CNRS, URA 2906, 91191 Gif sur Yvette, France, the [¶]Joint Genome Institute, United States Department of Energy, Walnut Creek, California 94598, the ^{||}Institut Jean-Pierre Bourgin, UMR 1318 INRA-AgroParisTech, INRA Versailles-Grignon, Route de Saint Cyr, F-78026 Versailles, France, and the ^{**}Department of Plant and Microbial Biology, University of California, Berkeley, California 94720

The photoprotective processes of photosynthetic organisms involve the dissipation of excess absorbed light energy as heat. Photoprotection in cyanobacteria is mechanistically distinct from that in plants; it involves the orange carotenoid protein (OCP), a water-soluble protein containing a single carotenoid. The OCP is a new member of the family of blue light-photoactive proteins; blue-green light triggers the OCP-mediated photoprotective response. Here we report structural and functional characterization of the wild type and two mutant forms of the OCP, from the model organism *Synechocystis* PCC6803. The structural analysis provides high resolution detail of the carotenoid-protein interactions that underlie the optical properties of the OCP, unique among carotenoid-proteins in binding a single pigment per polypeptide chain. Collectively, these data implicate several key amino acids in the function of the OCP and reveal that the photoconversion and photoprotective responses of the OCP to blue-green light can be decoupled.

The capture of light energy for oxygenic photosynthesis is arguably one of the most important metabolic processes on earth. It is also inherently risky; the absorbance of excess light energy beyond what can be used in photosynthesis can result in photooxidative damage to the organism. Consequently, photosynthetic organisms have evolved protective mechanisms to dissipate excess captured energy. In plants, one of these mechanisms involves the membrane-embedded chlorophyll-protein

antenna of Photosystem II, the light-harvesting complex (for reviews, see Refs. 1–4). Under saturating light conditions, the decrease of the lumen pH activates the xanthophyll cycle (5, 6) and the protonation of PsbS, a Photosystem II subunit (7). Conformational changes in the light-harvesting complex, modifying the interaction between chlorophyll molecules and carotenoids and allowing thermal dissipation, are also involved in this mechanism (8–10). Energy dissipation is accompanied by a diminution of Photosystem II-related fluorescence emission, also known as non-photochemical quenching (or NPQ; more specifically qE), which usually serves as a measure of the dissipation process.

Although the photoprotective mechanism of plants is well studied, only recently have mechanisms for photoprotection in the cyanobacteria been discovered (11–17). One of these occurs at the water-soluble light-harvesting antenna (the phycobilisome) and involves a novel photosensory protein, the orange carotenoid protein (13, 18–20). Most cyanobacterial species contain the OCP⁵ (21, 22), and in these organisms, it is constitutively expressed and is also up-regulated under extreme conditions, such as high light, iron starvation, and salt stress (18, 23–25). The OCP-mediated photoprotective mechanism is completely distinct from any known in plants and algae; it involves the absorption of blue-green light, which induces a shift in the absorbance properties of the OCP; visibly, the protein changes from orange to red (photoconversion). The structural basis of this photoconversion is unknown, but it appears to be a result of changes in both the protein and the carotenoid (19). The red, photoactive form of the protein induces the dissipation of energy from the phycobilisome as heat. This results in a measurable decrease (quenching) of phycobilisome fluorescence known as nonphotochemical quenching.

The OCP is of particular interest because it is the only photosensory protein characterized to date that uses a carotenoid as the chromophore. More broadly speaking, it is also a new member of the family of blue light-photoactive proteins; blue-green light is a ubiquitous environmental signal that activates a functionally diverse range of bacterial proteins, such as photoactive yellow protein (PYP) (26, 27) and those containing LOV

[§]The on-line version of this article (available at <http://www.jbc.org>) contains supplemental Table 1 and Figs. 1–4.

The atomic coordinates and structure factors (codes 3MG1, 3MG2, and 3MG3) have been deposited in the Protein Data Bank, Research Collaboratory for Structural Bioinformatics, Rutgers University, New Brunswick, NJ (<http://www.rcsb.org/>).

¹The work of these authors was supported by grants from l'Agence Nationale de la Recherche (Program CAROPROTECT) from CNRS and the Commissariat à l'Energie Atomique (Saclay, France).

²The work of these authors was performed under the auspices of the United States Department of Energy's Office of Science, Biological and Environmental Research Program, and the University of California, Lawrence Berkeley National Laboratory under Contract DE-AC02-05CH11231, Lawrence Livermore National Laboratory under Contract DE-AC52-07NA27344, and National Science Foundation Grant MCB-085170.

³Present address: Lawrence Berkeley National Laboratory, Berkeley, CA 94720.

⁴To whom correspondence should be addressed: 2800 Mitchell Dr., Walnut Creek, CA 94598. Tel.: 925-296-5691; Fax: 925-296-5752; E-mail: ckerfeld@berkeley.edu.

⁵The abbreviations used are: OCP, orange carotenoid protein; PYP, photoactive yellow protein; ECN, echinenone; TLS, translation, libration, screw; LOV, light, oxygen, or voltage; BLUF, blue light sensing using flavin; HMM, hidden Markov model; MES, 4-morpholineethanesulfonic acid; Wat, water; WT, wild type.

(28–31) or BLUF domains (32–35). Recent data available from genome sequencing as well as structural and functional characterization of these sensory proteins and their relatives have revealed that they share some general features in the structural basis of photoresponsiveness and signal transduction (36, 37).

Because the OCP is one of the few examples of a carotenoid-binding protein that is water-soluble and that contains only a single carotenoid molecule per polypeptide chain, it is an ideal system for the study of carotenoid-protein interactions. Mutant forms of the OCP, which can be made in *Synechocystis* PCC 6803 (hereafter referred to as *Synechocystis*), enable dissection of the role of individual amino acids in binding and in tuning the spectral properties of the carotenoid as well as their role in photoconversion and photoprotection. The 2.1 Å crystal structure of the OCP, from *Arthrospira maxima*, was reported in 2003, prior to an understanding of its function (38). Subsequent studies of the OCP in the model organism *Synechocystis* revealed its role in photoprotection (13, 18, 19). Here we report the 1.65 Å crystal structure of the WT OCP and of two OCP mutants from *Synechocystis*. The structural and functional characterization of OCP point mutants identified key roles for specific amino acids (Trp¹¹⁰, Tyr⁴⁴, and Arg¹⁵⁵) and demonstrated that the processes of photoconversion and nonphotochemical quenching can be decoupled. In addition, comparison of the *Synechocystis* and *A. maxima* OCP structures enabled identification of structurally conserved water molecules that may play a functional role. Finally, multiple structures of the OCP considered in the context of structure-function studies of other blue light-photoactive proteins reveal some interesting parallels and inform new hypotheses about the structural basis of the photoprotective function of the OCP.

EXPERIMENTAL PROCEDURES

Culture Conditions—*Synechocystis* wild type and mutants were grown photoautotrophically in a modified BG11 medium (39) containing twice the amount of sodium nitrate. Cells were kept in a rotary shaker (120 rpm) at 30 °C, illuminated by fluorescent white lamps giving a total intensity of about 30–40 $\mu\text{mol photons m}^{-2} \text{s}^{-1}$ under a CO₂-enriched atmosphere. The cells were maintained in the logarithmic phase of growth and were collected at OD_{800 nm} = 0.6–0.8. For OCP isolation, *Synechocystis* cells were grown in 3-liter Erlenmeyer flasks in a rotary shaker under a light intensity of 90–100 $\mu\text{mol photons m}^{-2} \text{s}^{-1}$. The cells were harvested at an OD_{800 nm} of 0.8–1.

Construction of OCP *Synechocystis* Mutants—To obtain single OCP mutants, wild type *Synechocystis* cells were transformed by a plasmid containing the mutated OCP gene (*slr1963*) with a C-terminal His tag and the hypothetical gene *slr1964* interrupted by a spectinomycin and streptomycin (Sp/Sm) resistance cassette (9). The point mutations Y44S, Y44F, W110F, and R155L were obtained by changing one or two nucleotides in the *slr1963* gene by site-directed mutagenesis using the QuikChange XL site-directed mutagenesis kit (Stratagene) and synthetic oligonucleotides (all of the oligonucleotides used in this work are described in supplemental Table 1). To obtain double OCP mutants overexpressing the mutated OCP, the mutated *slr1963* gene was cloned in an overexpressing plasmid in which the *slr1963* gene is under the control of the

psbAII promoter. The construction of the plasmid was described in Ref. 19. The plasmids containing the mutated *slr1963* genes under the control of the *psbAII* promoter were used to transform single OCP mutants of *Synechocystis* by double recombination (supplemental Fig. 1).

To confirm the introduction of the different mutations in the genomic *Synechocystis* DNA and complete segregation of mutants, PCR analysis and digestion by specific restriction enzymes were performed. Supplemental Fig. 2A shows that amplification of the genomic region containing the *slr1963* and *slr1964* genes (in the *psbAII* locus (lanes 1–4) or in the *slr1963* locus (lanes 5–9) using the synthetic psba1 and psba2 oligonucleotides or car6 and car7 oligonucleotides gave fragments of 1.5 or 2.2 kb, respectively, in the wild type and of 3.5 and 4.3 kb, respectively, in the mutants containing the antibiotic cassettes. No traces of the wild type fragment were detected in the mutants, indicating complete segregation. The presence of the different mutations was detected by digestion with restrictions enzymes (supplemental Fig. 2, B and C). The presence of the Y44S and W110F mutation was confirmed by the appearance of the supplemental NheI restriction site and the disappearance of the KpnI restriction site, respectively. Digestion of the amplified DNA fragments by BsmI indicated the presence of the R155L mutation. The presence of the mutations was confirmed by DNA sequencing. The construction of the His-tagged OCP, the overexpressing His-tagged OCP, His-tagged W110S OCP, and the overexpressing His-tagged W110S OCP were described in Ref. 19.

Purification of the Orange Carotenoid Protein—The purification of *Synechocystis* OCP was performed as previously described (19). Briefly, mutant cells (1 mg/ml chlorophyll) in Tris-HCl, pH 8, buffer were broken in dim light using a French press. The membranes were pelleted, and the supernatant was loaded on a column of nickel-Probond resin (Invitrogen). The OCP was further purified on a Whatman DE-52-cellulose column. Additional details of the purification are described in Ref. 19. The protein was stored in the dark at 4 °C.

Absorbance and Fluorescence Measurements—Cell absorbance was monitored with an UVIKONXL spectrophotometer (SECOMAN, Alès). Chlorophyll content was determined in methanol using the extinction coefficient at 665 nm of 79.24 mg ml⁻¹ cm⁻¹. The orange to red photoconversion was monitored in a Specord S600 spectrophotometer (Analyticjena, France) during illumination of the OCP with 1200 $\mu\text{mol photons m}^{-2} \text{s}^{-1}$ of blue-green light (400–550 nm) at 12 °C. Cell fluorescence was monitored with a pulse amplitude modulated fluorometer (101/102/103-PAM; Walz, Effelrich, Germany). All measurements were carried out in a stirred cuvette of 1-cm diameter at growth temperature (32 °C). Cells were preadapted to low irradiance of blue-green light (400–550 nm, 80 $\mu\text{mol photons m}^{-2} \text{s}^{-1}$) for about 1 min; then fluorescence quenching was induced by 740 $\mu\text{mol photons m}^{-2} \text{s}^{-1}$ of blue-green light for about 200 s. Saturating pulses (2000 $\mu\text{mol photons m}^{-2} \text{s}^{-1}$) were applied to measure the maximal fluorescence levels, $F'_{m,m}$, in light-adapted samples. Application of such pulses that transiently close all of the Photosystem II centers serves to distinguish between photochemical quenching and non-photochemical quenching.

Structural Insights into Cyanobacterial Photoprotection

OCP Immunodetection—Total cell protein was analyzed by SDS-PAGE on 12% polyacrylamide, 2 M urea (supplemental Fig. 3) in a Tris/MES system (40). The OCP protein was detected by a polyclonal antibody against OCP (18).

Carotenoid Characterization—Carotenoids were extracted from OCP preparations as described previously (41). Liquid chromatography-mass spectrometry analysis was performed as described in Ref. 42.

Sequence Analysis—The OCP logo was produced using an alignment of 28 OCP orthologs (reciprocal best BLAST hits to *Synechocystis* OCP) generated in Tcoffee. The hmmer package of tools on the MobyE EBI Web site server was used to generate an HMM from the alignment. The HMM was built using hmmbuild and then calibrated using hmmcalibrate. The Logo-Mat-M server was used to generate the HMM logo from the HMM.

Crystallization and Structure Determination—Wild type and mutant *Synechocystis* OCP were crystallized at 18 °C by the hanging drop vapor diffusion method over reservoir solutions identified from a screen of >1000 crystallization conditions. Because of the lack of appreciable effect of ambient light in triggering photoconversion of the OCP, no special precautions were taken to avoid room light. Wild type OCP (3.8 mg/ml 10 mM Tris, pH 7.7) was crystallized in drops containing 2 μ l of protein plus 1 μ l of reservoir solution (100 mM sodium acetate, pH 5.0, 10% polyethylene glycol 8000). Y44S OCP (3.3 mg/ml 10 mM Tris, pH 7.7) was crystallized in drops containing 2 μ l of protein and 1 μ l of reservoir solution (0.2 M CaCl₂, 18% polyethylene glycol 3350). R155L OCP (2.6 mg/ml 10 mM Tris, pH 7.7) was crystallized in drops containing 2 μ l of protein plus 0.5 μ l of reservoir solution (100 mM sodium acetate, pH 5.0, 10% polyethylene glycol 3350, and 2% glycerol). Protein concentration was measured using the Bradford protein assay (Bio-Rad).

For data collection, crystals were rapidly transferred into reservoir solutions supplemented with 25% glycerol, mounted into nylon loops, and frozen by placing directly into the cryostream of nitrogen gas. Diffraction data were collected at Lawrence Berkeley's Advanced Light Source, beamlines 8.2.1 and 5.02. The diffraction data were integrated and scaled with DENZO and SCALEPACK using HKL2000 (43). The wild type and both OCP mutants crystallized in space group P3₂ with two molecules in the asymmetric unit.

Structures were solved by molecular replacement using PHASER (44) implemented in CCP4 (45), and refinement was performed with phenix.refine (46) and REFMAC5 (47) using iterative cycles of positional and atomic B-factor refinement and model building with $2F_o - F_c$ and $F_o - F_c$ maps in COOT (48). During the final stages of refinement, NCS restraints were released in the structures of the wild type and R155L mutant to allow for slight differences in the monomers. TLS refinement was performed for the wild type and R155L structures. Four TLS domains were chosen using the TLSMD server corresponding to residue ranges 4–72, 73–169, 170–243, and 244–320.

In all three structures, there was some disorder at the N and C termini and in the linker region between the two domains, so these regions were not modeled. The refined wild type OCP structure (1.65 Å resolution) contains residues 3–164 and 171–

312 (chain A) and residues 3–164 and 171–312 (chain B). The Y44S mutant OCP (2.65 Å resolution) contains residues 4–163 and 172–312 (chain A) and residues 4–163 and 171–312 (chain B). The R155L mutant OCP (1.70 Å) contains residues 4–164 and 170–312 (chain A) and residues 3–164 and 170–312 (chains B). Electron density maps for each of the three models were well featured for the echinenone (ECN), enabling modeling at the final stages of refinement. Alternate conformations for side chains were visible in the relatively high resolution wild type and R155L models; these we modeled manually. Waters were modeled using the automatic solvent detection function in phenix.refine and checked manually in COOT. Additional crystallography statistics are listed in Table 1.

Analysis of the Structures—The stereochemistry of the final refined models were analyzed by MolProbity (49). Least squares root mean square deviation for comparison of different structures was performed with LSQKAB (50). Protein interfaces were analyzed using PDBSUM (51), PISA (52) and Profunc (53) servers at the European Bioinformatics Institute. Intraprotein aromatic-sulfur and aromatic-aromatic interactions were identified with the Protein Interaction Calculator (54), and protein-carotenoid interactions were defined by LigPlot (55). Figures were prepared with PyMOL (56).

Conserved Waters in the *Synechocystis* and *Arthrospira* OCP Structures—Structurally conserved water molecules were identified after superimposing the structures in the graphics program O (57) and then identifying overlapping waters within a 0.7 Å cut-off.

Size Exclusion Chromatography—Purified *Synechocystis* OCP was injected to a Superdex 75 HR 10/30 column (Amersham Biosciences) equilibrated with 40 mM Tris-HCl, pH 8, 150 mM NaCl. The Akta fast protein liquid chromatography system is equipped with a UV detector at 280 nm and was running at a flow rate of 0.5 ml/min. The gel filtration standard (Bio-Rad) included thyroglobulin (670 kDa), bovine γ -globulin (158 kDa), chicken ovalbumin (44 kDa), equine myoglobin (17 kDa), and bovine serum albumin (66 kDa). The standards were separated under the same conditions with and without OCP.

RESULTS AND DISCUSSION

Purification and Carotenoid Content of Wild Type and Mutant OCP—For purification of the OCP for structural and functional studies, His-tagged overexpressing OCP mutant strains of *Synechocystis* were constructed. The expressed protein was purified by nickel affinity and ion exchange chromatography (19). Analysis of the carotenoid content of the mutant proteins revealed that they contained a mixture of 3'-hydroxyechinenone, echinenone (ECN), and zeaxanthin (Table 2 and supplemental Fig. 4), as previously observed in strains overexpressing WT OCP (42). The relative content of each carotenoid varied, depending on the quantity of OCP present in the cell and on the mutation. With the exception of the OCP with a modified Trp¹¹⁰, in which 3'-hydroxyechinenone was the principal carotenoid detected, echinenone was the most abundant carotenoid present in OCP isolated from overexpressing strains. The presence of zeaxanthin varied from 6 to 30%. In darkness or dim light, the OCP isolated from all of the mutant strains appeared orange, and their absorption spectra were only

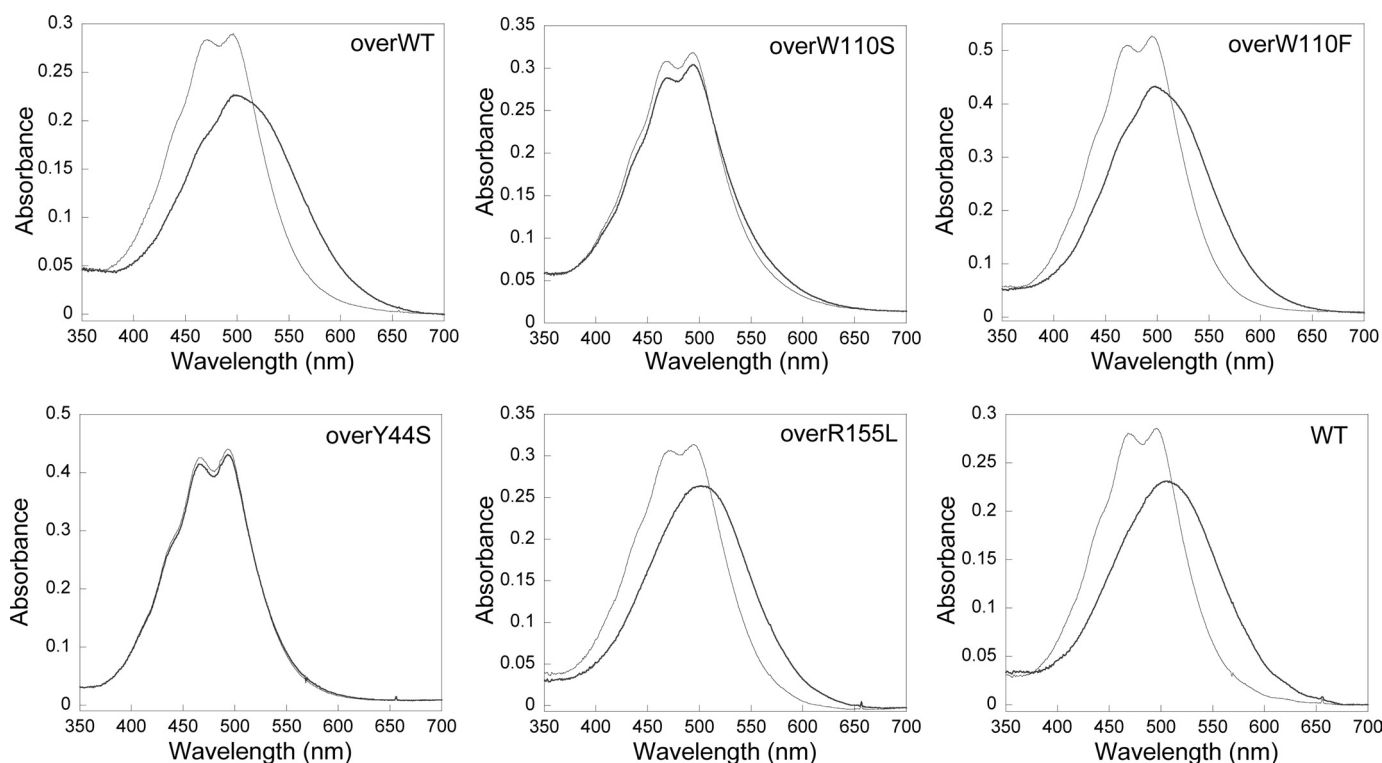


FIGURE 1. **Photoactivity of the isolated OCP preparations.** Shown are absorbance spectra of the orange (gray line) and red (heavy black line) forms of OCP isolated from the overexpressing His-tagged WT OCP strain (*overWT*), from the overexpressing His-tagged W110S OCP strain (*overW110S*), from the overexpressing His-tagged W110F OCP strain (*overW110F*), from the overexpressing His-tagged Y44S OCP strain (*overY44S*), from the overexpressing His-tagged R155L OCP strain (*overR155L*), and from the His-tagged WT strain (*WT*). To obtain the spectrum of the red, activated form, the isolated OCP was illuminated with $1200 \mu\text{mol photons m}^{-2} \text{s}^{-1}$ of blue light at 12°C for 5 min.

slightly different (Fig. 1). In some mutants (especially Y44S OCP), a spectrally distinct minor fraction containing more zeaxanthin eluted at slightly lower salt concentration, suggesting that the zeaxanthin-containing OCP detached more easily from the ion exchange column (data not shown). Because the zeaxanthin-OCP is inactive (42), this fraction was not used for further studies. Upon illumination with blue-green light, the WT OCP (containing only 3'-hydroxyechinenone (Table 2) was completely photoconverted to a red form (absorption maxima at 500–510 nm), whereas the OCP isolated from the overexpressing strain (containing 14% zeaxanthin) was not completely photoconverted (absorption maximum 498 nm) (Fig. 1) (42).

Structure of *Synechocystis* OCP—The structure of wild type *Synechocystis* OCP was solved by molecular replacement using a monomer of the *A. maxima* OCP (38) as a search model and refined to 1.65 \AA with a final R/R_{free} of 16.2/19.1%. The *Synechocystis* OCP was then used as a search model in molecular replacement to solve the crystal structures of the R155L and Y44S *Synechocystis* OCP mutants at 1.7 and 2.7 \AA resolution, respectively. Data and refinement statistics are given in Table 1.

The OCP consists of two domains (Fig. 2A), an N-terminal helical domain (residues 19–165; Pfam09150), composed of two four-helix bundles. The N-terminal domain of the OCP is the only known example of this protein fold. In contrast, the C-terminal domain (residues 193–311) is a member of the NTF2 (nuclear transport factor 2) superfamily (Pfam02136), which is found in a wide range of organisms. The NTF2 domain is a mixed α/β -fold; in the OCP, it comprises a five-stranded

β -sheet core flanked by three α -helices, (αK , αL , and αM). The N- and C-terminal domain are joined by a 28-amino acid linker that is the most variable region of primary structure among OCP orthologs (Fig. 3). Because of disorder, the first several residues of the linker (~ 164 – 171) could not be modeled in any of the three structures, suggesting that the region is flexible. The *Synechocystis* OCP structure closely resembles that of *A. maxima* (superimposing with a root mean square deviation of 0.55 \AA over 301 α -carbon atoms), reflecting the similarity (83% identical) of their primary structures. Indeed, the primary structure of all OCP orthologs is strongly conserved (21).

The three *Synechocystis* OCP structures were also similar to that of *A. maxima* OCP in that each contained two molecules in the crystallographic asymmetric unit arranged as an approximate antiparallel dimer (Fig. 4A). The dimerization interface in all four structures is similar, involving mainly the N-terminal domain. It contains 14 hydrogen bonds, two salt bridges (between Arg²⁷ and Asp¹⁹), and two water molecules that are conserved in both the *A. maxima* and *Synechocystis* OCP structures. The amount of surface area buried in the dimerization, $\sim 1100 \text{ \AA}^2/\text{monomer}$, exceeds the threshold value proposed to discriminate between a presumably biologically relevant interface and a crystal contact (856 \AA^2) (58). Because of the repeated observations of this interface in the different OCP structures, its size, and the precedent for functionally relevant oligomeric state changes in other blue light-responsive proteins (33, 59), we considered the likelihood that the OCP dimer is functionally relevant. The *A. maxima* OCP has been reported to be a dimer in gel filtration (38). However, the *Synechocystis* OCP eluted as

TABLE 1

X-ray data collection and refinement statistics

One crystal was used for each structure. Values in parentheses are for the highest resolution shell. NA, not applicable.

	Wild type	Y44S	R155L
Data collection			
Space group	P3 ₂	P3 ₂	P3 ₂
Cell dimensions			
<i>a</i> , <i>b</i> , <i>c</i> (Å)	82.94, 82.94, 87.63	83.19, 83.19, 87.97	82.68, 82.68, 86.57
α , β , γ (degrees)	90, 90, 120	90, 90, 120	90, 90, 120
Beamline	ALS 8.2.1	ALS 8.2.1	ALS 5.0.2
Wavelength	1.0000	1.0000	1.0000
Resolution (Å)	50-1.65 (1.71-1.65)	50-2.65 (2.74-2.65)	50-1.7 (1.76-1.70)
<i>R</i> _{merge}	6.3 (34.0)	12.9 (68.7)	7.2 (51.6)
<i>I</i> / <i>s</i> (<i>I</i>)	35.1 (3.7)	12.0 (2.1)	19.0 (6.5)
Completeness (%)	99.3 (93.9)	100 (100)	99.0 (98.1)
Redundancy	6.4 (3.8)	5.6 (5.3)	5.7 (5.7)
Refinement			
Resolution (Å)	37.5-1.65	41.6-2.65	41.3-1.70
No. of reflections	80,620	19,717	71,837
<i>R</i> _{work} / <i>R</i> _{free}	16.18/19.05	19.41/25.92	15.33/19.07
No. of atoms			
Protein	4667	4580	4653/8262 ^a
Water	736	150	648
ECN	82	82	82/190 ^a
Glycerol	12	0	42/74 ^a
Average isotropic <i>B</i> -factors (Å ²)			
Protein	26.45	35.33	24.23/26.17 ^a
Water	40.97	32.15	37.25
ECN	24.08	28.81	15.34/17.31 ^a
Glycerol	31.08	NA	26.75 ^a /26.56 ^a
Root mean square deviations			
Bond lengths (Å)	0.006	0.003	0.014
Bond angles (degrees)	1.015	0.701	1.433

^aIncludes hydrogens used in refining the Protein Data Bank structure.

a monomer in gel filtration in both its resting (orange; Fig. 5) and photoactivated form (data not shown). Moreover, thermodynamic calculations of the energy of binding of the intermolecular interface in both the *A. maxima* and *Synechocystis* dimers suggest that it is not a stable assembly. Furthermore, if the OCP dimer was functionally relevant, it would be expected that residues in the intermolecular interface would be conserved in the primary structure of the OCP; however, only three of the 22 amino acids making up the dimerization interface are absolutely conserved among OCP orthologs. It appears more likely that the repeatedly observed dimerization in the crystals is an artifact of the relatively high protein concentration and/or conditions used for crystallization.

Structural Parallels to Other Blue Light Photoreceptor Proteins—In the past 5 years, while we have gained an understanding of the function of the OCP, a substantial amount of new structural, functional, and sequence information has been obtained for other blue light photoreceptors, such as BLUF and LOV domains and PYP (which, like the LOV domain, is a member of the PAS structure superfamily). BLUF and LOV domains are found covalently connected to their effector domains or can be present as isolated modules with their effector domains encoded separately. Interestingly, common mechanistic principles underlying response to blue-green light in PYP and the functionally diverse BLUF and LOV domains are emerging (36). LOV and BLUF domains as well as PYP share a common β -sheet core flanked by helices. The interaction of the chromophore with the β -sheet originates a signal that is propagated to the effector region of the protein through side chain movements and changes in hydrogen bonding patterns. The OCP is similar to these other blue light-responsive proteins in that the core of its C-terminal domain, which hydrogen-bonds to the

carotenoid, is a β -sheet flanked by helices. Likewise, accumulating genomic sequence data suggests that modularity is part of the evolutionary history of the OCP; open reading frames encoding isolated N- and C-terminal domains of the OCP are observed in numerous cyanobacterial genomes (21). Accordingly, in interpreting the specific features of the OCP structure in the context of function, we consider if there is evidence of structural features similar to those that underlie the general principles of signal transduction known from PYP and BLUF and LOV domains.

Carotenoid-Protein Interactions in the *Synechocystis* OCP and Implications for Function—The OCP isolated directly from *A. maxima* and *Synechocystis* cultures contains the carotenoid 3'-hydroxyechinenone, whereas the *Synechocystis* mutant overexpressing the OCP contains mainly ECN (Table 2) (42). The photoprotective activity of the ECN-containing OCP is comparable with that containing 3'-hydroxyechinenone, indicating that the hydroxyl group in 3'-hydroxyechinenone, which potentially hydrogen bonds to the N-terminal domain in the *A. maxima* OCP, is not critical for function (42). Electron density maps calculated using phases from the partially refined model of the *Synechocystis* OCP without carotenoid were of high quality, enabling *de novo* building of the ECN molecule in each monomer. The conformation of the ECN in the two *Synechocystis* OCP monomers is identical (within the range of coordinate error) and is similar to that of 3'-hydroxyechinenone in the *A. maxima* OCP (root mean square deviation 0.2 Å over 41 atoms; Fig. 4B). As in the *A. maxima* OCP, the carotenoid in the *Synechocystis* OCP spans the N- and C-terminal domains; it is almost entirely buried; only 4% of the ECN is solvent-exposed. In the N-terminal domain, the ECN is nestled between the two four-helix bundles (Fig. 2A). In the C-terminal

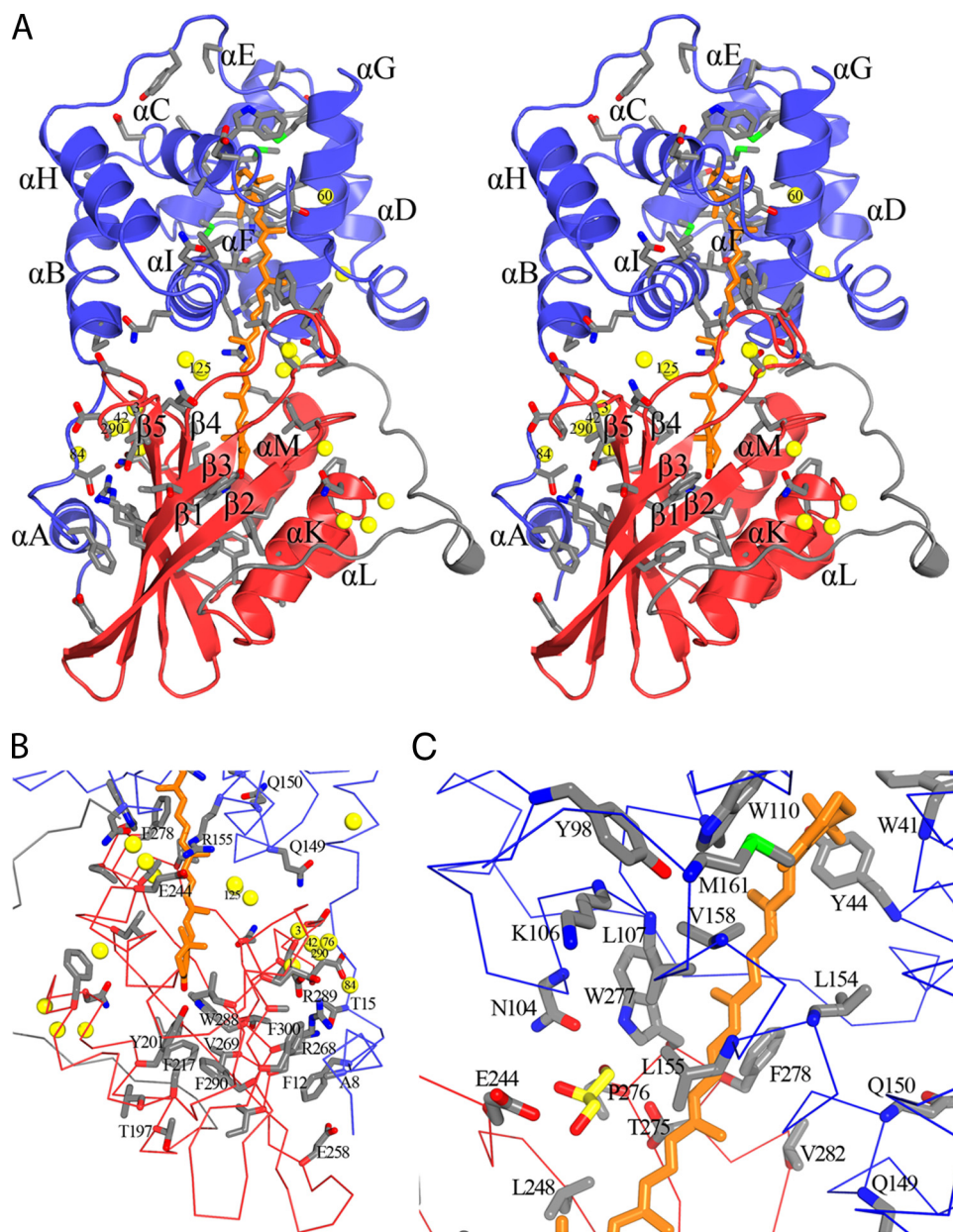


FIGURE 2. Structure of the *Synechocystis* OCP. *A*, stereo representation of the overall structure of the *Synechocystis* OCP. The N-terminal domain is colored blue; the C-terminal domain is shown in red, and the carotenoid is represented by sticks (orange). The linker region between the two domains is shown in gray. The side chains of conserved residues among the OCP orthologs are shown as gray sticks with polar atoms colored (oxygen in red; nitrogen in blue; sulfur in green). Structurally conserved water molecules are shown as yellow spheres. Water molecules discussed throughout the text are numbered. *B*, the N-terminal and central interfaces between the N- and C-terminal domains of the OCP, colored as in *A*. *C*, structure of the central interface in the R155L OCP mutant. The glycerol molecule is shown in yellow sticks with oxygen atoms colored red.

domain, it occupies a cleft formed between the β -sheet and α M and α K (Fig. 2, *A* and *B*). The keto group of the ECN hydrogen-bonds with the absolutely conserved amino acids Tyr²⁰¹ (α Y) and Trp²⁸⁸ of the central strand (β 4) of the β -sheet (Fig. 2*B*); the hydrogen-bonding distances are 2.6 and 2.9 Å, respectively. The hydrogen bond to Tyr²⁰¹ is a relatively short hydrogen bond; these are often functionally important (60, 61). Short hydrogen bonds between the chromophore and the protein are central to a network of hydrogen bonds in PYP that are critical to its photocycle (62). In the OCP, the orientation of the Tyr²⁰¹ side chain appears to be stabilized via aromatic interactions

(63), with two absolutely conserved phenylalanine side chains (Phe²¹⁷ and Phe²⁹⁰), whereas the orientation of Trp²⁸⁸ may be in part stabilized by an aromatic sulfur interaction with the strongly conserved Met²⁰². The importance of the hydrogen bonds between the protein and the carotenoid for the function of the OCP is underscored by studies of zeaxanthin-containing OCP; zeaxanthin lacks an oxygen atom for hydrogen bonding, and zeaxanthin-OCP is not photoactive, nor is it able to induce fluorescence quenching under strong blue-green light (42). Changes in these hydrogen bonds upon photoactivation could be communicated through the β -sheet or to the surface of the OCP via residues hydrogen-bonded to Tyr²⁰¹ and Trp²⁸⁸ (Fig. 2*B*). For example, the backbone of Tyr²⁰¹ is hydrogen-bonded to the backbone of Thr¹⁹⁷ (α K), which is surface-exposed. Through backbone atoms, Tyr²⁰¹ is hydrogen-bonded (3.1 Å) to Leu²⁰⁵ (α K), which is hydrogen-bonded (3.0 Å), also through backbone atoms, to surface-exposed Asn²⁰⁸. The backbone of Trp²⁸⁸ (β 4) forms two hydrogen bonds to the backbone of Val²⁶⁹ (β 3; 2.8 and 2.9 Å). Through an aromatic-sulfur interaction with Met²⁰² and its hydrogen bonding, Trp²⁸⁸ has an additional potential interaction with the α K helix. The multiple hydrogen bonding pathways to the α K helix are notable because it is part of the C-terminal domain in the OCP (α K, β 2, β 3, β 4) that shows some structural similarity to the phycobilisome core linker protein, APLc (19); mimicking the interaction of the linker with the phycobilisome core could allow this region to

interact with the chromophores, providing a pathway for energy dissipation. Alternatively, or in addition, changes in the chromophore upon absorption of light could influence interactions between the N- and C-terminal domains of the OCP, which, by revealing new sites for interprotein interaction, could be functionally relevant. These hypotheses are discussed below in the context of analogous mechanisms in other blue light-responsive proteins.

The residues within 3.9 Å of the carotenoid are shown in Fig. 4*A*. Of these 24 residues, eight are highly conserved aromatic amino acids (Fig. 3). All of these, except the two in the C-ter-

Structural Insights into Cyanobacterial Photoprotection

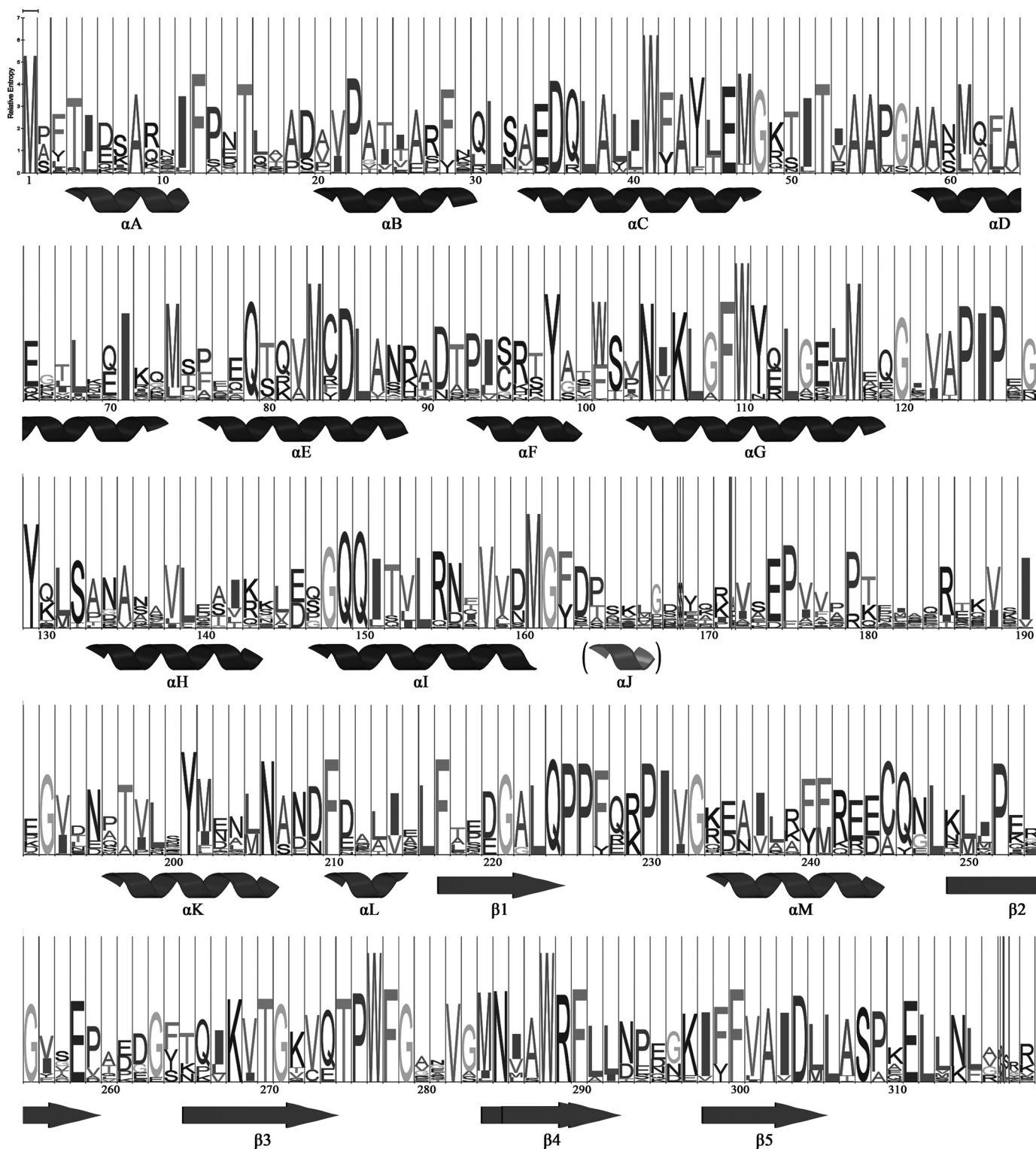


FIGURE 3. **Primary and secondary structure of the OCP.** HMM sequence logo derived from the primary structure of OCP orthologs (reciprocal best BLAST hits to the sequence of *Synechocystis* OCP) with secondary structure elements based on the *Synechocystis* wild type structure. The linker region is composed of residues 166–192. αJ is found in the *A. maxima* OCP structure, but because of disorder in this region in the *Synechocystis* OCP electron density, it was not modeled.

minimal domain that hydrogen-bond to the carotenoid (Tyr²⁰¹ and Trp²⁸⁸), are located in the N-terminal domain, where they form a dense constellation around the carotenoid. A tendency for carotenoids to be surrounded by aromatic amino acids in all structurally characterized photosynthetic pigment protein

complexes has been noted. The aromatic side chains are thought to influence selectivity for carotenoid binding (64), and the pi-pi stacking interactions provide an important noncovalent force in binding carotenoid to the protein (65). Both the orientation of the aromatic side chains and their distance to the

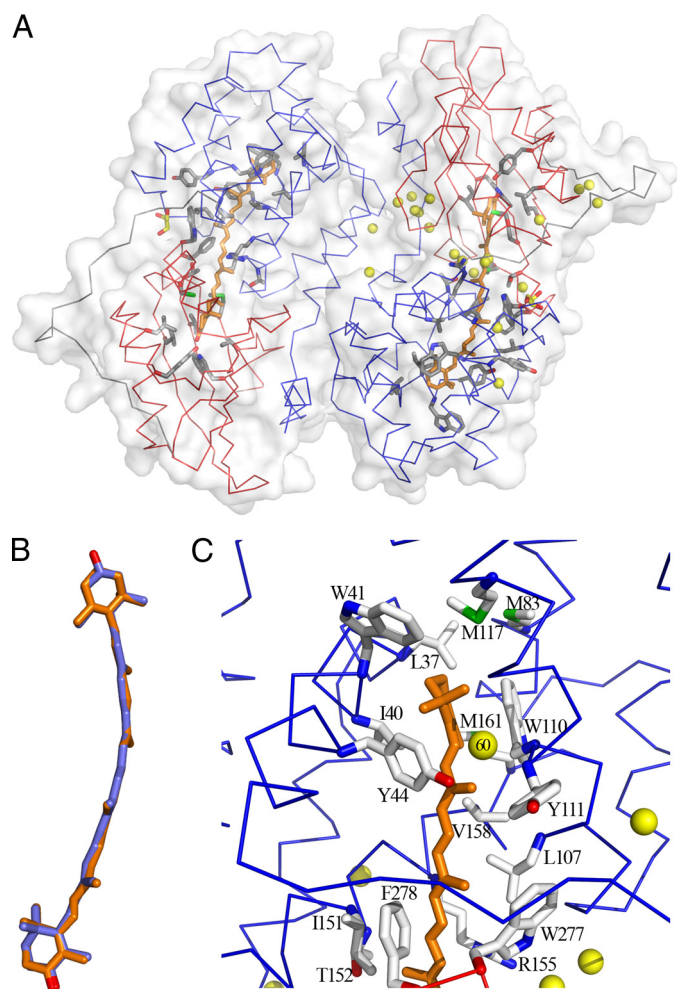


FIGURE 4. Carotenoid-protein interactions in the OCP and comparison of carotenoid conformations between *A. maxima* and *Synechocystis* OCP. A, the two molecules of *Synechocystis* wild type OCP in the crystallographic asymmetric unit are shown. The two domains are colored as in Fig. 2, and the molecule on the right contains the structurally conserved water molecules. Residues within 3.9 Å of the carotenoid are shown as gray sticks with polar atoms colored as in Fig. 2. Glycerol molecules are shown as yellow sticks. B, superposition of the ECN (orange) and 3'-hydroxyechinenone (blue) from the *Synechocystis* and *A. maxima* OCP structures. C, close-up of the carotenoid-protein interactions in the N-terminal domain; side chains and water molecules discussed throughout the text are labeled.

carotenoid have been proposed to be functionally significant (65). In the N-terminal domain of the OCP, absolutely conserved Trp⁴¹, Trp¹¹⁰, and Tyr⁴⁴ surround the terminal ring of the ECN (Fig. 4C). Several structural features in the N-terminal domain suggest that it may be important in intra- and/or inter-protein interactions mediating the photoprotective function of the OCP. A water molecule conserved among the wild type OCP structures (Wat⁶⁰) and the side chains of Tyr⁴⁴ (which displays alternate side chain conformations) and Trp⁴¹ surround one of only two regions in the OCP in which the carotenoid is solvent-exposed (Fig. 4C). Movement of either of these side chains and/or of the conserved water molecule could increase surface accessibility of the carotenoid. Likewise, conserved methionine residues in this region could facilitate structural rearrangements in activation of the OCP. The sulfur atoms of three absolutely conserved methionine residues (83, 117, and 161) make intraprotein aromatic-sulfur interactions

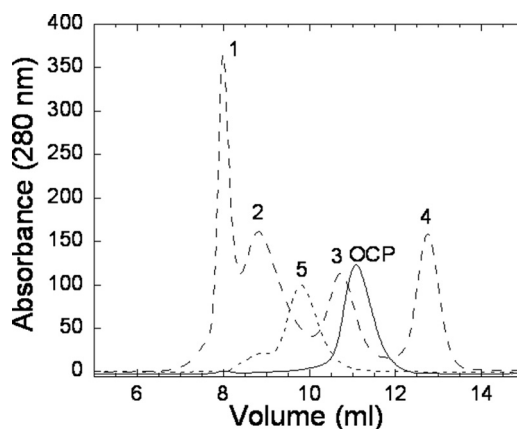


FIGURE 5. Gel filtration of *Synechocystis* OCP. Shown are size exclusion chromatograms of OCP and standards (shifted up) labeled 1 for thyroglobulin (670 kDa), 2 for γ -globulin (158 kDa), 3 for ovalbumin (43 kDa), 4 for myoglobin (17.6 kDa), and 5 for bovine serum albumin (66 kDa; additional standard). OCP was eluted at 11.2 ml after ovalbumin (elution at 10.8 ml), which has a molecular mass of 43 kDa. Experiments were performed with and without OCP mixed with standards.

TABLE 2
Carotenoid content of *Synechocystis* WT and mutant *Synechocystis* OCP

Strains ^a	Carotenoid ^b content			Phenotype ^c
	Echinenone	OH-echinenone	Zeaxanthin	
	%	%	%	
OverR155L	61	29	9	NoQ O/R
OverY44S	73	8	19	NoQ O
OverW110F	23	48	29	Q O/R
OverW110S	24	76		NoQ O
WT	5	95		Q O/R
OverWT	70	16	14	Q O/R

^a The "over-" prefix denotes an overexpressing strain.

^b See supplemental Fig. 4 for the carotenoid structures.

^c Q, fluorescence quenching observed; NoQ, no fluorescence quenching observed; O/R, photoconverts between orange and red forms; O, does not convert to red form.

(66) with Trp⁴¹ and Trp¹¹⁰ side chains (Fig. 4C). Methionine side chains, because of their conformational flexibility, are often involved in protein conformational changes or molecular recognition (67, 68). Photoactivation in BLUF domains provides an example. In the BLUF domain of BlrP1 (33), a conserved methionine residue undergoes a large positional displacement, which changes its interaction with a glutamine (or a tryptophan in AppA (34)) residue to accommodate the latter's movement in response to the absorption of light (33, 34, 69).

Characterization of *Synechocystis* OCP point mutants was used to probe the role of single amino acids in the photoprotective function of OCP. Although the effect of changing these amino acids in photoconversion (from orange to red) can be monitored by measuring the spectral change in the OCP absorbance in response to blue-green light (Fig. 1), the degree of photoprotection is measured by analyzing fluorescence quenching of mutants (Fig. 6). The OCP-related photoprotective mechanism involves an increase of energy dissipation as heat in the phycobilisome. This results in a decrease (quenching) of the phycobilisome fluorescence that can be detected a PAM fluorometer (13, 70). Mutants impaired in OCP-mediated photoprotection have reduced blue light-induced quenching. To verify that any reduction in fluorescence quenching in the mutants was not the result of reduced OCP levels, a second

Structural Insights into Cyanobacterial Photoprotection

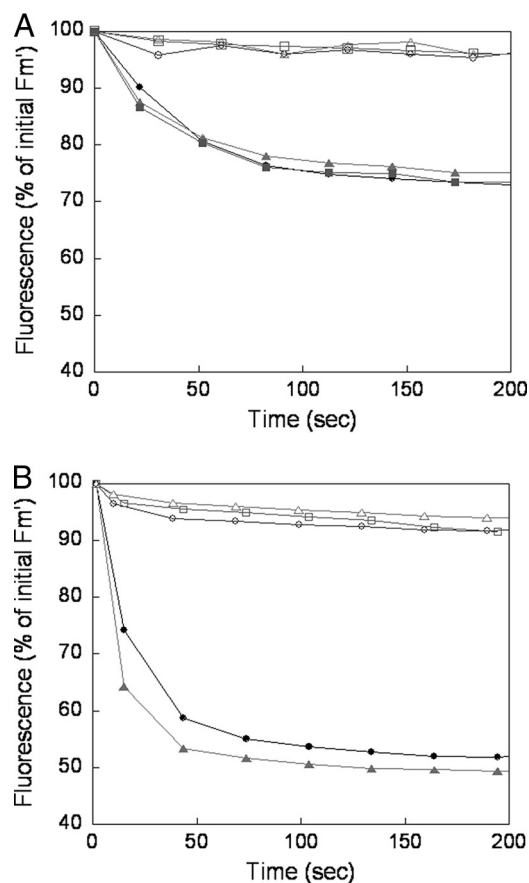


FIGURE 6. Blue-green light-induced fluorescence quenching in single OCP mutants. Low light-adapted cells ($80 \mu\text{mol photons m}^{-2} \text{s}^{-1}$) (at $3 \mu\text{g/ml}$ chlorophyll) of WT (closed circles) and of simple mutants Y44S (open squares), Y44F (closed squares), W110S (open triangles), W110F (closed triangles), and R155L (open circles) (A) and overexpressing WT OCP (closed circles), W110S OCP (open triangles), W110F OCP (closed triangles), Y44S OCP (open squares), and R155L OCP (open circles) (B) were illuminated with high intensities ($740 \mu\text{mol photons m}^{-2} \text{s}^{-1}$) of blue-green light (400–550 nm). Fluorescence yield changes were detected with a PAM fluorometer, and saturating pulses were applied to measure maximal fluorescence levels (F_m).

mutation to induce the overexpression of the OCP was made in each mutant. By measuring OCP content in the overexpressing mutants, we verified that the phenotypic changes observed were not due to a reduced level of the OCP in the cells (supplemental Fig. 3).

Previously, we have shown that changing Trp¹¹⁰ to a serine abolishes the photoprotective function of OCP (19). To test the hypothesis that the aromatic character of the side chain in this position is critical to function, we substituted Trp¹¹⁰ with phenylalanine. In the W110F mutant, OCP incompletely photoconverts to the red form (Fig. 1). The conversion is incomplete because about 30% of the protein contained zeaxanthin and was consequently not photoactive. However, in the single and double (overexpressing) W110F mutants, the level of photoprotection was similar to the wild type and the overexpressing wild type strains, respectively (Fig. 6), confirming the importance of the role of the aromatic amino acid in this position. In the single and double W110F mutant, the OCP photoconversion (Fig. 1) and photoprotective function (Fig. 6) are similar to those of wild type, confirming the importance of the role of the aromatic amino acid in this position.

Likewise, changing Tyr⁴⁴ to a serine results in a lack of photoconversion (Fig. 1) and fluorescence quenching (Fig. 6); however, changing Tyr⁴⁴ to another aromatic amino acid (Y44F) did not affect photoconversion or photoprotection (Figs. 1 and 6). Thus, like Trp¹¹⁰, the aromatic character of this side chain appears to be essential to the OCP function. We crystallized the Y44S OCP and solved the structure. Other than increased solvent accessibility to the carotenoid due to the substitution of a smaller side chain at this position, there are no substantial differences between the structure of the Y44S mutant and the wild type OCP. This suggests either that solvent accessibility at this site is not important to the function of the OCP, or it is the ability to modulate the accessibility to solvent that is important for function. As expected, the conserved water molecule (Wat⁶⁰) that hydrogen-bonds to the Tyr⁴⁴ is not visible in the structure of the Y44S OCP, nor is there ordered solvent hydrogen bonding to the serine side chain; however, the resolution limit of this structure is relatively low (2.7 Å). Crystallization of the Y44S mutant was more challenging than the wild type. The wild type and mutant OCP protein preparations were of comparable purity, possibly indicating that the lower resolution may be a result of higher overall flexibility of the Y44S mutant protein, and therefore conformational heterogeneity, in the mutant OCP.

*Additional Structural Implications for Function of the OCP—*In the model of the mechanism for OCP photoprotective function, the OCP interacts with the core of the phycobilisome. Presumably to dissipate excitation energy, the carotenoid must approach the phycobilisome core for energy transfer from its chromophores. This could also be facilitated by conformational changes in the OCP that would reversibly allow additional carotenoid exposure. This hypothesis is supported by Fourier transform infrared spectroscopy data that indicate that there are secondary structure changes upon photoconversion by blue light (19). Recent observations that glutaraldehyde and high concentrations of sucrose or glycerol abolish OCP-mediated non-photochemical quenching in *Synechocystis* (14, 71) are consistent with a role of protein motion in OCP photoprotective function.

Alterations in the interactions between the N- and C-terminal domain may be important in the OCP photoprotective function by serving as a means for propagating a signal or exposing sites for interprotein interactions. The interaction between the N- and C-terminal domains can be divided into two regions (Fig. 2, A and B) we refer to as the N-terminal and the central interfaces.

The N-terminal interface between the N- and C-terminal domains buries 947 and 775 \AA^2 of the N- and C-terminal domains, respectively. It involves the first 19 amino acids of the N-terminal domain (which contains a short helix, αA) that extends away from the N-terminal domain to interact with the solvent-exposed face of the β -sheet (Fig. 2B). Many of the amino acids making up this face of the sheet and the terminal loop are absolutely conserved among OCP orthologs (Gln²²⁴, Glu²⁵⁸, Lys²⁶⁸, Thr²⁷⁹, Arg²⁸⁹, Phe³⁰⁰, Asp³⁰⁴, Leu³⁰⁶, Ser³⁰⁸ and Glu³¹¹; Fig. 2B). As noted above, light absorption by the carotenoid in the OCP and consequent alteration of the hydrogen bonding of the carotenoid to the C-terminal domain could

be propagated to the N-terminal extension (Fig. 2B). A paradigm for this type of signal transduction is observed in LOV domains, in which the signal emanating from the β -sheet core is propagated to a helix from a remote part of the protein that is packed against the core in the resting state. For example, in phototropin, photoactivation of the FAD chromophore alters its hydrogen bonding to the protein, which is communicated through the β -sheet, culminating in the displacement of a short α -helix, $J\alpha$, that is associated with the LOV domain, stimulating kinase activity (72–75). The associated Fourier transform infrared spectroscopy shift patterns during this LOV domain photoactivation are similar to those observed for activation of the OCP (19).

In the OCP, structurally conserved water molecules could also play a role in signal transduction. Conserved water molecules are known to have various roles in protein structure and function (76); for example, in rhodopsin, water molecules are proposed to be involved in spectral tuning and regulating activity (77). Displacement of conserved water molecules is thought to be important in effecting conformational changes in signal transduction (78–80). In the N-terminal interface, there are six structurally conserved water molecules (Wat¹, Wat³, Wat⁴², Wat⁷⁶, Wat⁸⁴, and Wat²⁹⁰) in a depression on the protein surface beneath a semicircular ridge formed by interaction of the N-terminal extension and the β -sheet. Wat¹ and Wat³ are partially buried and have relatively low B-factors (18.1 and 15.7 Å²). Movement of the N-terminal extension would increase the solvent accessibility of these water molecules as well as the solvent accessibility of the conserved amino acids on this face of the β -sheet.

Alternatively, a change in the interaction of the N- and C-terminal domain of the OCP across the central interface could also be involved in the OCP photoprotective mechanism. Given that the two domains are joined by a linker (residues 163–193) that appears to be flexible (the electron density for this region was poorly ordered in all three *Synechocystis* OCP structures described here), alterations in the conformation of the linker could result in changes in the central interface between the N- and C-terminal domains, increasing the exposure of the carotenoid for interaction with the phycobilisome.

The central interface buries 628 and 723 Å² of the N- and C-terminal domains, respectively. It contains eight structurally conserved water molecules (Fig. 2B). Two of these (Wat²⁰ and Wat¹²⁵) are within 3.9 Å of the carotenoid and are found in the second region of the OCP in which the carotenoid is slightly solvent exposed. The interface is stabilized by four hydrogen bonds, including two formed between the pairs of conserved residues Asn¹⁰⁴ and Trp²⁷⁷ and Arg¹⁵⁵ and Glu²⁴⁴. The latter salt bridge also flanks the surface depression in which the carotenoid is solvent-exposed. Both Arg¹⁵⁵ and Glu²⁴⁴ hydrogen-bond to a structurally conserved water molecule (Wat²⁰⁰). Breakage of this salt bridge and the concomitant movement of the side chains would increase the solvent accessibility of the carotenoid and of the conserved water molecules, exposing new hydrogen bonding partners for other molecules. A change in the solvent accessibility of the chromophore and related rearrangements in hydrogen bonding and associated changes in

electrostatic potential and shape complementarity are known to be important for the photocycle of PYP (26).

To examine the role of this interdomain salt bridge for OCP function, Arg¹⁵⁵ was changed to a leucine. Upon illumination with blue-green light (400–550 nm) at 10 °C, the orange His-tagged R155L OCP (containing traces of zeaxanthin; Table 2) was completely photoconverted to the red form (Fig. 1). The spectrum of the red form of the R155L OCP was similar to that of the WT OCP. The maxima of both spectra were at 500–510 nm, but the WT red OCP is slightly broader in the red region of the spectrum. However, the R155L mutant under illumination was unable to induce fluorescence quenching (Fig. 6). This indicates that photoconversion and quenching are discrete events and suggests that changes in the interaction of the N- and C-terminal domain at the central interface are critical to the structural changes that allow the OCP dissipate excess energy from the phycobilisome. The 1.7 Å crystal structure of the R155L mutant revealed no significant differences from the wild type in overall structure of the OCP (root mean square deviation of 0.2 Å over the α -carbon backbones of the dimers). A glycerol molecule necessary to the crystallization is found in the space formerly occupied by the arginine side chain (Fig. 2C) and hydrogen bonds (2.7 Å) to the Glu²⁴⁴ side chain. The glycerol compensates for the R155L mutation and stabilizes the interface between the N- and C-terminal domains, possibly immobilizing it and thus preventing conformational changes.

CONCLUSION

The 1.65 Å crystal structure of the *Synechocystis* OCP will be valuable to ongoing genetic and spectroscopic studies of OCP-mediated photoprotection in cyanobacteria. The structural and functional characterization of the mutants reported here are the first steps toward dissecting out the roles of single amino acids and perhaps structural water molecules in the function of OCP. The mutants confirm previous hypotheses about the role of aromatic amino acids and conformational changes in signal transduction in the function of the OCP. Furthermore, the R155L mutation provides the first evidence that photoconversion and photoprotection are discrete events in the mechanism of OCP. Further studies of this mutant with Raman and infrared spectroscopy will provide information about the carotenoid-protein interaction in solution, and the changes in the protein induced by light provide key information for elucidating the precise details of the photoprotective mechanism of OCP. Likewise, efforts are under way to crystallize the photoactivated form of the OCP; this structure should reveal changes in the carotenoid and protein that underlie the spectral differences between the orange and red forms.

Signaling proteins tend to be modular and constructed by combining sensor and effector domains (81). Like other blue light photoreceptors, the OCP is modular, and there are some similarities between its C-terminal domain and those of other blue light sensory domains, including ligand/cofactor binding within its α/β -fold. Recently, it has been noted that there are parallels emerging between the mechanism of light sensing in BLUF and LOV domains; the structural basis of function of other blue light photoreceptor proteins can be used to guide the

Structural Insights into Cyanobacterial Photoprotection

development of new hypotheses about the mechanism of OCP function. If the OCP proves to share similar features in photo-activation and signaling, it will enhance our understanding of the evolution of bacterial mechanisms to detect and respond to blue light in their environment.

Acknowledgments—We acknowledge Seth Axen for assistance in preparation of the figures. The carotenoid composition of the OCP was analyzed on the “Plateau Technique Spécifique de Chimie du Végétal” of Institut Jean-Pierre Bourgin.

REFERENCES

1. Demmig-Adams, B. (1990) *Biochim. Biophys. Acta* **1020**, 1–24
2. Horton, P., Ruban, A. V., and Walters, R. G. (1996) *Annu. Rev. Plant Physiol. Plant Mol. Biol.* **47**, 655–684
3. Müller, P., Li, X. P., and Niyogi, K. K. (2001) *Plant Physiol.* **125**, 1558–1566
4. Niyogi, K. K. (1999) *Annu. Rev. Plant Physiol. Plant Mol. Biol.* **50**, 333–359
5. Gilmore, A. M., and Yamamoto, H. Y. (1993) *Photosynth. Res.* **35**, 67–78
6. Yamamoto, H. Y. (1979) *Pure Appl. Chem.* **51**, 639–648
7. Li, X. P., Björkman, O., Shih, C., Grossman, A. R., Rosenquist, M., Jansson, S., and Niyogi, K. K. (2000) *Nature* **403**, 391–395
8. Pascal, A. A., Liu, Z., Broess, K., van Oort, B., van Amerongen, H., Wang, C., Horton, P., Robert, B., Chang, W., and Ruban, A. (2005) *Nature* **436**, 134–137
9. Ruban, A. V., Berera, R., Illoaia, C., van Stokkum, I. H., Kennis, J. T., Pascal, A. A., van Amerongen, H., Robert, B., Horton, P., and van Grondelle, R. (2007) *Nature* **450**, 575–578
10. Ruban, A. V., Rees, D., Pascal, A. A., and Horton, P. (1992) *Biochim. Biophys. Acta* **1102**, 39–44
11. El Bissati, K., Delphin, E., Murata, N., Etienne, A., and Kirilovsky, D. (2000) *Biochim. Biophys. Acta* **1457**, 229–242
12. Rakhimberdieva, M. G., Stadnichuk, I. N., Elanskaya, I. V., and Karapetyan, N. V. (2004) *FEBS Lett.* **574**, 85–88
13. Wilson, A., Ajlani, G., Verbavatz, J. M., Vass, I., Kerfeld, C. A., and Kirilovsky, D. (2006) *Plant Cell* **18**, 992–1007
14. Scott, M., McCollum, C., Vasil'ev, S., Crozier, C., Espie, G. S., Krol, M., Huner, N. P., and Bruce, D. (2006) *Biochemistry* **45**, 8952–8958
15. Ihalainen, J. A., D'Haene, S., Yermenko, N., van Roon, H., Arteni, A. A., Boekema, E. J., van Grondelle, R., Matthijs, H. C., and Dekker, J. P. (2005) *Biochemistry* **44**, 10846–10853
16. Yermenko, N., Kouril, R., Ihalainen, J. A., D'Haene, S., van Oosterwijk, N., Andrizhivskaya, E. G., Keegstra, W., Dekker, H. L., Hagemann, M., Boekema, E. J., Matthijs, H. C., and Dekker, J. P. (2004) *Biochemistry* **43**, 10308–10313
17. Havaux, M., Guedeny, G., He, Q., and Grossman, A. R. (2003) *Biochim. Biophys. Acta* **1557**, 21–33
18. Wilson, A., Boulay, C., Wilde, A., Kerfeld, C. A., and Kirilovsky, D. (2007) *Plant Cell* **19**, 656–672
19. Wilson, A., Punginelli, C., Gall, A., Bonetti, C., Alexandre, M., Routaboul, J. M., Kerfeld, C. A., van Grondelle, R., Robert, B., Kennis, J. T., and Kirilovsky, D. (2008) *Proc. Natl. Acad. Sci. U.S.A.* **105**, 12075–12080
20. Kirilovsky, D. (2007) *Photosynth. Res.* **93**, 7–16
21. Kerfeld, C. A., Alexandre, M., and Kirilovsky, D. (2009) in *Carotenoids: Physical, Chemical, and Biological Functions and Properties* (Landrum, J., ed) pp. 3–17, CRC Press, Inc.
22. Boulay, C., Abasova, L., Six, C., Vass, I., and Kirilovsky, D. (2008) *Biochim. Biophys. Acta* **1777**, 1344–1354
23. Hihara, Y., Kamei, A., Kanehisa, M., Kaplan, A., and Ikeuchi, M. (2001) *Plant Cell* **13**, 793–806
24. Singh, A. K., Elvitigala, T., Bhattacharyya-Pakrasi, M., Aurora, R., Ghosh, B., and Pakrasi, H. B. (2008) *Plant Physiology* **148**, 467–478
25. Fulda, S., Mikkat, S., Huang, F., Huckauf, J., Marin, K., Norling, B., and Hagemann, M. (2006) *Proteomics* **6**, 2733–2745
26. Genick, U. K., Borgstahl, G. E., Ng, K., Ren, Z., Pradervand, C., Burke, P. M., Srajer, V., Teng, T. Y., Schildkamp, W., McRee, D. E., Moffat, K., and Getzoff, E. D. (1997) *Science* **275**, 1471–1475
27. Hellingwerf, K. J., Hendriks, J., and Gensch, T. (2003) *J. Phys. Chem. A* **107**, 1082–1094
28. Crosson, S., Rajagopal, S., and Moffat, K. (2003) *Biochemistry* **42**, 2–10
29. Losi, A., and Gärtner, W. (2008) *Proc. Natl. Acad. Sci. U.S.A.* **105**, 7–8
30. Swartz, T. E., Tseng, T. S., Frederickson, M. A., Paris, G., Comerchi, D. J., Rajashekar, G., Kim, J. G., Mudgett, M. B., Splitter, G. A., Ugalde, R. A., Goldbaum, F. A., Briggs, W. R., and Bogomolni, R. A. (2007) *Science* **317**, 1090–1093
31. Losi, A. (2004) *Photochem. Photobiol. Sci.* **3**, 566–574
32. Gomelsky, M., and Klug, G. (2002) *Trends Biochem. Sci.* **27**, 497–500
33. Barends, T. R., Hartmann, E., Griese, J. J., Beitlich, T., Kirienko, N. V., Ryjenkov, D. A., Reinstein, J., Shoeman, R. L., Gomelsky, M., and Schlichting, I. (2009) *Nature* **459**, 1015–1018
34. Jung, A., Reinstein, J., Domratcheva, T., Shoeman, R. L., and Schlichting, I. (2006) *J. Mol. Biol.* **362**, 717–732
35. Metz, S., Jäger, A., and Klug, G. (2009) *J. Bacteriol.* **191**, 4473–4477
36. Losi, A. (2007) *Photochem. Photobiol.* **83**, 1283–1300
37. Möglich, A., Ayers, R. A., and Moffat, K. (2009) *Structure* **17**, 1282–1294
38. Kerfeld, C. A., Sawaya, M. R., Brahmamdam, V., Cascio, D., Ho, K. K., Trevithick-Sutton, C. C., Krogmann, D. W., and Yeates, T. O. (2003) *Structure* **11**, 55–65
39. Herdman, M., Delaney, S. F., and Carr, N. G. (1973) *J. Gen. Microbiol.* **79**, 233–237
40. Kashino, Y., Koike, H., and Satoh, K. (2001) *Electrophoresis* **22**, 1004–1007
41. Polívka, T., Kerfeld, C. A., Pascher, T., and Sundström, V. (2005) *Biochemistry* **44**, 3994–4003
42. Punginelli, C., Wilson, A., Routaboul, J. M., and Kirilovsky, D. (2009) *Biochim. Biophys. Acta* **1787**, 280–288
43. Otwinowski, Z., and Minor, W. (1997) *Methods Enzymol. A* **276**, 307–326
44. Read, R. J. (2001) *Acta Crystallogr. D Biol. Crystallogr.* **57**, 1373–1382
45. Collaborative Computational Project 4 (1994) *Acta Crystallogr. D Biol. Crystallogr.* **50**, 760–763
46. Adams, P. D., Grosse-Kunstleve, R. W., Hung, L. W., Ioerger, T. R., McCoy, A. J., Moriarty, N. W., Read, R. J., Sacchettini, J. C., Sauter, N. K., and Terwilliger, T. C. (2002) *Acta Crystallogr. D Biol. Crystallogr.* **58**, 1948–1954
47. Murshudov, G. N., Vagin, A. A., and Dodson, E. J. (1997) *Acta Crystallogr. D Biol. Crystallogr.* **53**, 240–255
48. Emsley, P., and Cowtan, K. (2004) *Acta Crystallogr. D Biol. Crystallogr.* **60**, 2126–2132
49. Davis, I. W., Murray, L. W., Richardson, J. S., and Richardson, D. C. (2004) *Nucleic Acids Res.* **32**, W615–W619
50. Kabsch, W. (1976) *Acta Crystallogr. A* **32**, 922–923
51. Laskowski, R. A. (2009) *Nucleic Acids Res.* **37**, D355–D359
52. Krissinel, E., and Henrick, K. (2007) *J. Mol. Biol.* **372**, 774–797
53. Laskowski, R. A., Watson, J. D., and Thornton, J. M. (2005) *Nucleic Acids Research* **33**, W89–W93
54. Tina, K. G., Bhadra, R., and Srinivasan, N. (2007) *Nucleic Acids Res.* **35**, W473–W476
55. Wallace, A. C., Laskowski, R. A., and Thornton, J. M. (1995) *Protein Engineering* **8**, 127–134
56. DeLano, W. L. (2002) *The PyMOL Molecular Graphics System*, DeLano Scientific LLC, Palo Alto, CA
57. Jones, T. A., Zou, J. Y., Cowan, S. W., and Kjeldgaard, M. (1991) *Acta Crystallogr. A* **47**, 110–119
58. Pongstingl, H., Henrick, K., and Thornton, J. M. (2000) *Proteins Struct. Funct. Genet.* **41**, 47–57
59. Nakasone, Y., Eitoku, T., Matsuoka, D., Tokutomi, S., and Terazima, M. (2006) *Biophys. J.* **91**, 645–653
60. Rajagopal, S., and Vishveshwara, S. (2005) *FEBS J.* **272**, 1819–1832
61. Cleland, W. W. (2000) *Arch. Biochem. Biophys.* **382**, 1–5
62. Anderson, S., Crosson, S., and Moffat, K. (2004) *Acta Crystallogr. D* **60**, 1008–1016
63. Burley, S. K., and Petsko, G. A. (1985) *Science* **229**, 23–28
64. Roszak, A. W., McKendrick, K., Gardiner, A. T., Mitchell, I. A., Isaacs,

- N. W., Cogdell, R. J., Hashimoto, H., and Frank, H. A. (2004) *Structure* **12**, 765–773
65. Mao, L., Wang, Y., and Hu, X. (2003) *J. Phys. Chem. B* **107**, 3963–3971
66. Reid, K. S., Lindley, P. F., and Thornton, J. M. (1985) *FEBS Lett.* **190**, 209–213
67. Pal, D., and Chakrabarti, P. (2001) *J. Biomol. Struct. Dyn.* **19**, 115–128
68. Gellman, S. H. (1991) *Biochemistry* **30**, 6633–6636
69. Yuan, H., Anderson, S., Masuda, S., Dragnea, V., Moffat, K., and Bauer, C. (2006) *Biochemistry* **45**, 12687–12694
70. El Bissati, K., and Kirilovsky, D. (2001) *Plant Physiol.* **125**, 1988–2000
71. Rakhimberdieva, M. G., Bolychevtseva, Y. V., Elanskaya, I. V., and Karapetyan, N. V. (2007) *FEBS Lett.* **581**, 2429–2433
72. Harper, S. M., Neil, L. C., and Gardner, K. H. (2003) *Science* **301**, 1541–1544
73. Koyama, T., Iwata, T., Yamamoto, A., Sato, Y., Matsuoka, D., Tokutomi, S., and Kandori, H. (2009) *Biochemistry* **48**, 7621–7628
74. Yamamoto, A., Iwata, T., Sato, Y., Matsuoka, D., Tokutomi, S., and Kandori, H. (2009) *Biophys. J.* **96**, 2771–2778
75. Alexandre, M. T., van Grondelle, R., Hellingwerf, K. J., and Kennis, J. T. (2009) *Biophys. J.* **97**, 238–247
76. Ball, P. (2008) *Chem. Rev.* **108**, 74–108
77. Pardo, L., Deupi, X., Dölker, N., López-Rodríguez, M. L., and Campillo, M. (2007) *ChemBiochem* **8**, 19–24
78. Angel, T. E., Chance, M. R., and Palczewski, K. (2009) *Proc. Natl. Acad. Sci. U.S.A.* **106**, 8555–8560
79. Angel, T. E., Gupta, S., Jastrzebska, B., Palczewski, K., and Chance, M. R. (2009) *Proc. Natl. Acad. Sci. U.S.A.* **106**, 14367–14372
80. Hofmann, K. P., Scheerer, P., Hildebrand, P. W., Choe, H. W., Park, J. H., Heck, M., and Ernst, O. P. (2009) *Trends Biochem. Sci.* **34**, 540–552
81. Pawson, T., and Nash, P. (2003) *Science* **300**, 445–452

Structural Determinants Underlying Photoprotection in the Photoactive Orange Carotenoid Protein of Cyanobacteria

Adjele Wilson, James N. Kinney, Petrus H. Zwart, Claire Punginelli, Sandrine D'Haene, François Perreau, Michael G. Klein, Diana Kirilovsky and Cheryl A. Kerfeld

J. Biol. Chem. 2010, 285:18364-18375.

doi: 10.1074/jbc.M110.115709 originally published online April 5, 2010

Access the most updated version of this article at doi: [10.1074/jbc.M110.115709](https://doi.org/10.1074/jbc.M110.115709)

Alerts:

- [When this article is cited](#)
- [When a correction for this article is posted](#)

[Click here](#) to choose from all of JBC's e-mail alerts

Supplemental material:

<http://www.jbc.org/content/suppl/2010/04/21/M110.115709.DC1>

This article cites 79 references, 16 of which can be accessed free at <http://www.jbc.org/content/285/24/18364.full.html#ref-list-1>